

# **In vacuo synthesis of single-layer Ni<sub>3</sub>(HITP)<sub>2</sub> on HOPG surface using metallo-organic precursor**

Chuyu Song<sup>†</sup>, Yifei Feng<sup>†</sup>, Henan Chen, Nian Lin\*

Department of Physics, The Hong Kong University of Science and Technology, Clear Water Bay, Hong Kong 999077, China

<sup>†</sup>These authors contributed equally to this work

\*Corresponding author: [phnlin@ust.hk](mailto:phnlin@ust.hk)

## Abstract

Single-layer conjugated metal–organic frameworks (SL c-MOFs) are predicated theoretically to host rich quantum phases. To date, however, the experimental synthesis has largely resulted in SL c-MOFs on metal substrates, whose intrinsic properties are strongly screened due to substrate hybridization. To overcome this obstacle, here we develop a method to grow clean SL c-MOF Ni<sub>3</sub>(HITP)<sub>2</sub> on a chemically inert substrate of highly oriented pyrolytic graphite (HOPG). By means of an ultra-high vacuum based multi-step protocol using nickel acetylacetonate [Ni(acac)<sub>2</sub>] precursor, we obtain continuous single-layer Ni<sub>3</sub>(HITP)<sub>2</sub>. Scanning tunneling microscopy reveals a well-defined hexagonal framework with a uniform azimuthal orientation rotated by approximately 30° with respect to the underlying graphite lattice. Furthermore, we control the growth of bilayer Ni<sub>3</sub>(HITP)<sub>2</sub> which features an unusual AA stacking configuration. This work establishes metallo-organic chemistry as an efficient route for integrating 2D c-MOFs onto inert substrates, which opens a new avenue for exploring the exotic quantum properties of SL c-MOFs.

## Introduction

Metal–organic frameworks (MOFs) are porous crystalline materials constructed from metal nodes and organic linkers [1,2]. Owing to exceptional structural tunability and versatile functionalities, MOFs have been studied extensively in the past three decades [3-5]. Among them, two-dimensional conjugated MOFs (2D c-MOFs) represent a unique type of 2D materials [6-14]. Specifically, theoretical predictions have envisioned that rich quantum phases can be realized in 2D c-MOFs such as quantum spin Hall state, quantum anomalous Hall state, Chern flat band, quantum spin liquids, etc.[15-26]. Most 2D c-MOF sample are in the form of thin films or multilayers with their thickness ranging from 1~2  $\mu\text{m}$  to 10 nm. Single layer (SL) 2D MOFs synthesized by the means of conventional “wet” chemistry are rarely reported. [27]. Considering the quantum phases are prone to inter-layer interactions, single-layer (SL) c-MOF samples are highly desirable. In this regard, on-surface coordination assembly on metal substrates offers an efficient approach for preparing SL-2D MOFs [28,29]. However, the strong screening of the metal substrate can obscure the intrinsic properties of the MOF.

Synthesizing SL c-MOFs on chemically inert substrates like graphene [30-32], h-BN [33,34], or other van der Waals materials [35] offers an effective approach to minimize substrate screening effects and preserve their intrinsic properties. Our previous studies have achieved SL c-MOFs on inert substrates of HOPG and MoS<sub>2</sub> [36,37]. Nevertheless, these systems are based on linker molecules that do not require dehydrogenation because dehydrogenation reactions on the inert substrates remain a significant challenge. In addition, metal atoms deposited on the inert substrates tend to aggregate into large clusters rather than dispersed as single atoms, which complicates the formation of large crystalline domains.

Here we demonstrate a strategy utilizing metallo-organic precursors of metal acetylacetonate complexes  $[\text{M}(\text{acac})_x]$  to synthesize SL c-MOFs on chemically inert substrates. The acetylacetonate ligand offers several distinct advantages [39-41]: (i) its

strong bidentate chelation stabilizes the metal center in a +2 oxidation state, preventing metal aggregation or reduction in the course of sublimation and deposition; (ii) the acac moiety undergoes clean thermal decomposition at moderate temperatures, producing only volatile byproducts (acetone, CO<sub>2</sub>) with no residue; and (iii) M(acac)<sub>x</sub> compounds can be sublimated at moderate temperatures, allowing for precise control over metal precursor delivery. These characteristics make acetylacetonates suitable for forming SL c-MOF on inert substrates.

Ni<sub>3</sub>(HITP)<sub>2</sub> is predicted to exhibit non-trivial quantum phase [42-44]. In this work, we demonstrate that Ni(acac)<sub>2</sub> enables controlled growth of single-layer Ni<sub>3</sub>(HITP)<sub>2</sub> on an HOPG substrate through a multi-step protocol. The resulting Ni<sub>3</sub>(HITP)<sub>2</sub> single layers exhibit good crystallinity with a homogenous orientation with respect to the graphite lattice. We also achieve controlled synthesis of a bilayer structure and identify an AA-stacked bilayer. We test the stability of the Ni<sub>3</sub>(HITP)<sub>2</sub> single layers and find that they retain the structural integrity after 350 °C heating and air exposure, making them accessible for device integration.

## Results and discussion

The multi-step growth protocol is illustrated in Figure 1. 2,3,6,7,10,11-hexaiminotriphenylene (HATP) linker molecules and Ni(acac)<sub>2</sub> precursors are co-deposited onto an HOPG substrate held at the room temperature (i). The substrate is then annealed at ~250 °C for 10 minutes (ii). At this temperature, the Ni(acac)<sub>2</sub> precursors are fragmented to release Ni<sup>2+</sup> ions and acac ligands. The acac ligands capture protons from the amino groups of HATP to form neutral Hacac molecules that desorb from the HOPG surface. The deprotonation converts HATP into its reactive form 2,3,6,7,10,11-hexaiminotriphenylene (HITP), which coordinate with the Ni<sup>2+</sup> ions, resulting in single-layer Ni<sub>3</sub>(HITP)<sub>2</sub> domains on the substrate (iii). The un-reacted Ni(acac)<sub>2</sub> precursors and the partially fragmented precursors aggregate as clusters, denoted as Ni(acac)<sub>x</sub> clusters. Figure 2a shows the representative sample

morphology of iii. One can see the hexagonal framework of the single-layer  $\text{Ni}_3(\text{HITP})_2$  formed on the left part of the image and three large clusters and two small cluster are at the edges of the  $\text{Ni}_3(\text{HITP})_2$  domains. The apparent size of the clusters is in the range of 6~7 nm laterally and 2.5~3.5 nm vertically (Figure S1a).

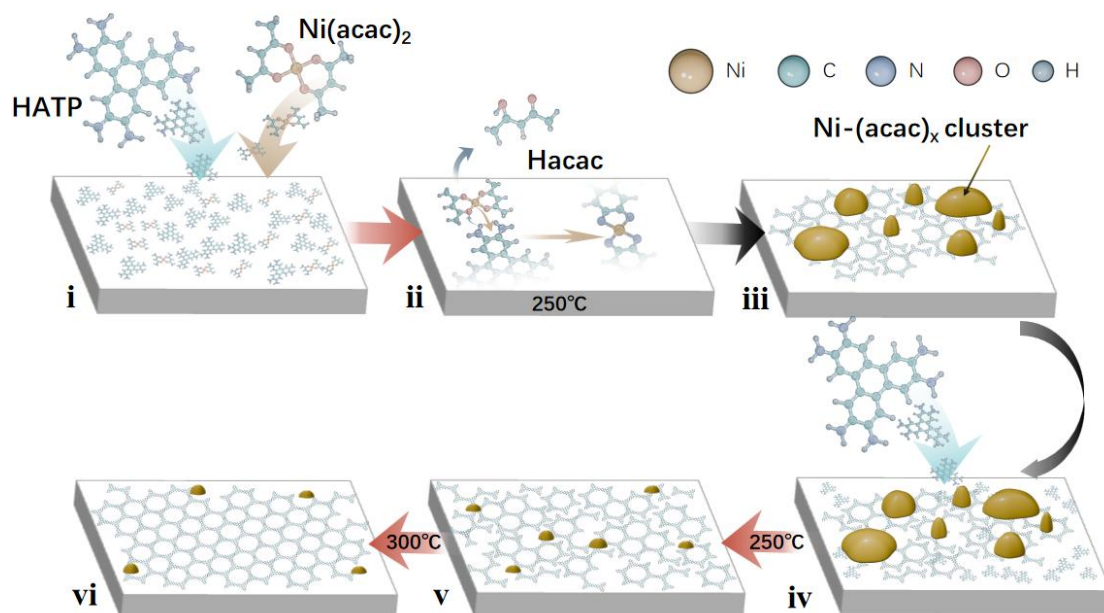


Figure 1. Schematic Illustration showing the multi-step growth process: (i) Co-deposition of HATP and  $\text{Ni}(\text{acac})_2$  precursors on HOPG; (ii) On-surface HATP deportation and  $\text{Ni}^{2+}$  coordination; (iii) Formation of  $\text{Ni}_3(\text{HITP})_2$  single layer together with  $\text{Ni}(\text{acac})_x$  clusters; (iv) Cycles of subsequent reaction with additional HATP; (v) Formation of single layer  $\text{Ni}_3(\text{HITP})_2$  composed of small domains; (vi) Formation of single layer  $\text{Ni}_3(\text{HITP})_2$  composed of large domains.

In the next step (iv), additional HATP are deposited on the sample, which is annealed at  $\sim 250$  °C for 10 minutes. This process is repeated several times. As a result of such cycles, more and more single-layer  $\text{Ni}_3(\text{HITP})_2$  domains are formed while the  $\text{Ni}(\text{acac})_x$  clusters are gradually reduced in size (5.0~5.5 nm laterally and 1.5~2.5 nm vertically) and in density (Figure S1b) (v). We propose, in these cycles, the  $\text{Ni}(\text{acac})_x$  clusters provide acac ligands to deprotonate the later supplied HATP molecules and  $\text{Ni}^{2+}$  ions to coordinate with the resultant HITP to form  $\text{Ni}_3(\text{HITP})_2$ . Presumably, the

repeating reactions recycle the unreacted and partially fragmented  $\text{Ni}(\text{acac})_2$  precursors.

When the  $\text{Ni-acac}_x$  clusters are nearly consumed, the single-layer  $\text{Ni}_3(\text{HITP})_2$  covers  $\sim 80\%$  of the surface (Figure 2b). Closer inspections reveal that the single layer is composed of small domains of  $\sim 10$  nm size. These domains are in the same azimuthal orientation (Figure S2) and separated by misalignment domain boundaries and defect lines. Presumably, different domains are formed out of different nucleation seeds in the growth process. To enlarge domain size, the sample is annealed at  $\sim 300$  °C for 10 minutes (vi). Figure 2c shows that the resultant single layer exhibits enlarged domains. The domains can reach a size of  $\sim 30$  nm, are more closely packed and better ordered. The misalignment domain boundaries and defect lines are reduced significantly.

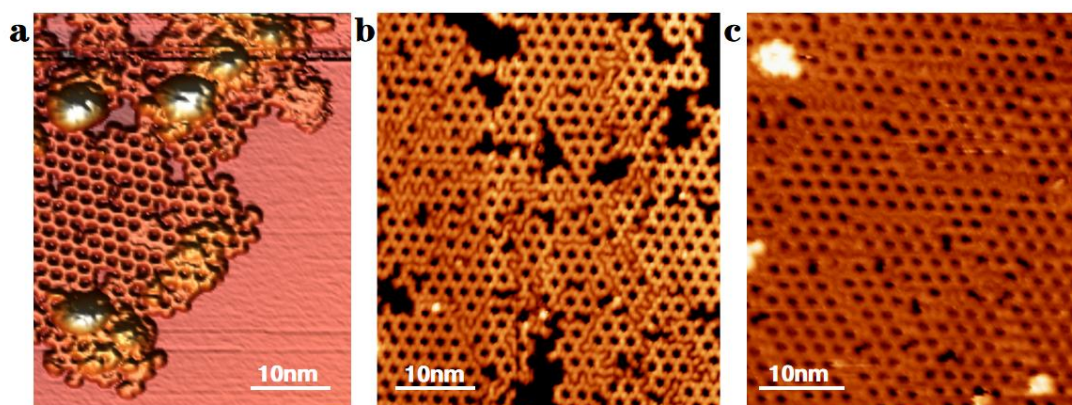


Figure 2. STM images showing the sample morphology of steps (iii), (v) and (vi) in the multi-step growth. (a) Single-layer  $\text{Ni}_3(\text{HITP})_2$  domains with  $\text{Ni}(\text{acac})_x$  clusters. (b) Single-layer  $\text{Ni}_3(\text{HITP})_2$  composed of small domains. (c) Single-layer  $\text{Ni}_3(\text{HITP})_2$  composed of large domains. Scanning parameters:  $V = -2$  V,  $I = 500$  pA.

We conducted series of controlled experiments to gain further insights into the growth mechanism. First, we co-deposited metallic nickel and HATP on the HOPG substrate held at room and elevated temperatures, respectively. Neither method yields  $\text{Ni}_3(\text{HITP})_2$ . Ni atoms form large clusters adhered at the steps of the HOPG substrate (Figure S3a), in contrast,  $\text{Ni}(\text{acac})_2$  aggregate as small clusters on the open terraces of

the HOPG substrate (Figure S3b). Presumably, the Ni atom clusters do not provide reactive agents to deprotonate HATP. Secondly, we co-deposited HATP and Ni(acac)<sub>2</sub> simultaneously on a HOPG held at high temperature (~300 °C). This method yields small pieces of Ni<sub>3</sub>(HITP)<sub>2</sub> at step edges of the HOPG substrate (Figure S4). This result suggests that the co-deposited Ni(acac)<sub>2</sub> and HATP at the hot substrate easily desorb from the substrate, which is unfavored for growing large Ni<sub>3</sub>(HITP)<sub>2</sub> domains. Finally, to test the substrate effects, we replace HOPG with a single crystal Au(111) as the substrate. Unlike those formed on HOPG, small domains of Ni<sub>3</sub>(HITP)<sub>2</sub> that are scattered and orientated in multiple directions are formed on the Au(111) substrate (Figure S5).

Figure 3a is a high-resolution STM image of the Ni<sub>3</sub>(HITP)<sub>2</sub> single layer, displaying a hexagonal framework. The red rhombus frame highlights the unit cell of Ni<sub>3</sub>(HITP)<sub>2</sub>. The lattice constant of the unit cell is 2.19±0.02 nm, which is consistent with the free-standing Ni<sub>3</sub>(HITP)<sub>2</sub> lattice constant [42,45]. The Ni atoms could not be resolved. This is attributed to charge delocalization due to strong conjugation of Ni<sub>3</sub>(HITP)<sub>2</sub>. The blue arrows indicate a<sub>1</sub> and a<sub>2</sub> crystallographic directions of the substrate graphite lattice, indicating that the Ni<sub>3</sub>(HITP)<sub>2</sub> lattice is rotated by 30° with respect to the underneath graphite atomic lattice. Figure 3b depicts a molecular model of the Ni<sub>3</sub>(HITP)<sub>2</sub> single layer on the graphite substrate. Note that the registration of Ni<sub>3</sub>(HITP)<sub>2</sub> on the graphite atomic lattice is tentative since the underneath graphite atoms could not be resolved simultaneously.

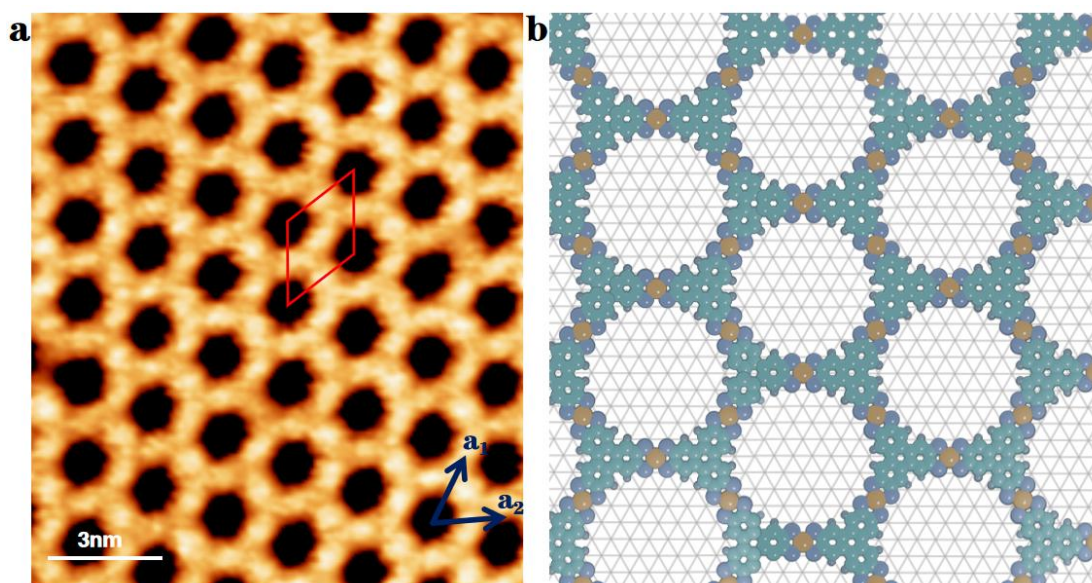


Figure 3.  $\text{Ni}_3(\text{HITP})_2$  single layer. (a) High-resolution STM image. The red rhombus frame highlights the unit cell and the blue arrows indicate  $a_1$  and  $a_2$  crystallographic directions of the underlying graphite atomic lattice. Scanning parameters:  $V = -2 \text{ V}$ ,  $I = 500 \text{ pA}$ . (b) Tentative molecular model of the  $\text{Ni}_3(\text{HITP})_2$  single layer adsorbed on the graphite lattice.

After forming the  $\text{Ni}_3(\text{HITP})_2$  single layer, depositing excessive HATP to react with the remaining  $\text{Ni}(\text{acac})_x$  clusters results in second layer  $\text{Ni}_3(\text{HITP})_2$  formed on top of the single layer. Figure 4a shows the two layers exhibit the same lattice orientation and lattice constant. Figure 4c is the cross-sectional height profile of line ABC in Figure 4a. In section AB, the peak-valley corrugation of the second layer aligns with that of the first layer as guided with the blue rulers, indicating an AA stacking configuration of the bilayer structure, as illustrated in Figure 4b. In section BC, the cross-sectional height profile reveals that the first layer is  $\sim 0.40 \text{ nm}$  above the HOPG substrate, and the second layer is  $\sim 0.35 \text{ nm}$  above the first layer. This value is a typical interlayer distance of van der Waals layer materials. Figure 4d shows a side view model of the bilayer structure.

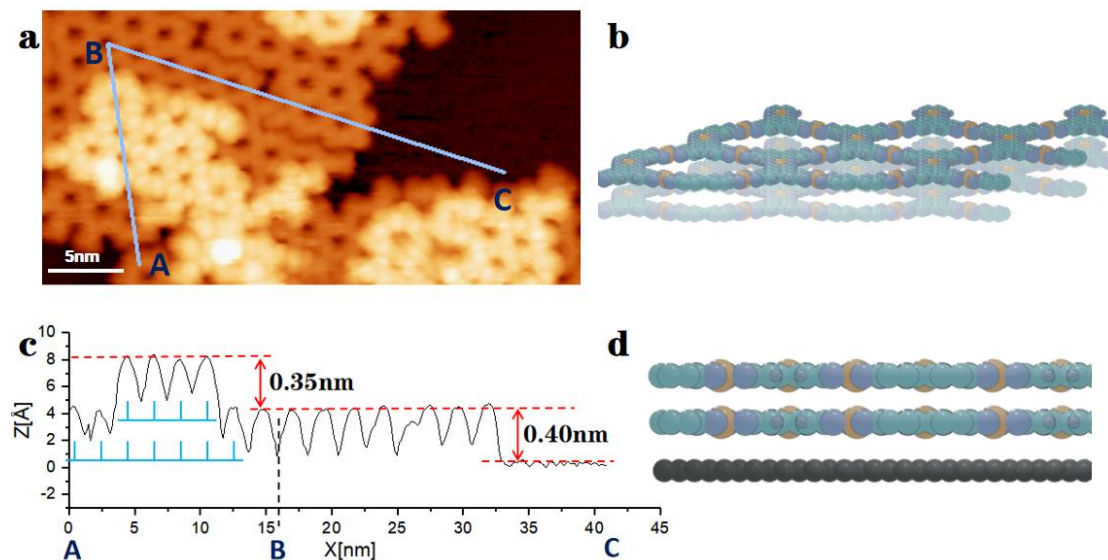


Figure 4. Bilayer  $\text{Ni}_3(\text{HITP})_2$  structure. (a) STM image. Scanning parameters:  $V = -2 \text{ V}$ ,  $I = 500 \text{ pA}$ . (b) AA stacking of the bilayer structure. (c) Cross-sectional height profile of ABC in (a), showing the AA-stacking alignment of the two layers and the inter-layer distance. (d) Side view model of the bilayer structure on graphite.

Last but not the least, we tested the structural stability of the  $\text{Ni}_3(\text{HITP})_2$  single layer. We found that after annealing at  $350 \text{ }^\circ\text{C}$  for 10 min, the framework structure remained intact (Figure S6a). We took the sample out of vacuum and exposed it to the ambient air for 30 minutes. After introducing the sample to vacuum and annealing at  $250 \text{ }^\circ\text{C}$  to remove the ambient adsorbates, the framework structure remained intact (Figure S6b). These results suggest that the  $\text{Ni}_3(\text{HITP})_2$  single layer is suitable for further processing and device integration.

## Conclusion

In summary, we have developed an effective method of using metallo-organic precursor to grow clean single layers c-MOF on an inert substrate. The multi-step growth protocol yields continuous c-MOF single layers with a uniform crystallographic orientation with respect to the underlying substrate lattice. This method highlights two key ingredients for forming c-MOF on the inert substrate,

namely, preventing metal aggregation and activating ligand deprotonation. We anticipate that this method is applicable for other metallo-organic precursors and other linker molecules. The bilayer growth offers promising prospect of using different precursors subsequently to grow layer-by-layer heterostructure c-MOFs. Considering the intrinsic properties of c-MOFs grown on inert substrates are preserved, these samples are suitable for fabricating c-MOF based devices.

## **Methods**

All measurements were conducted using an Omicron ultrahigh vacuum (UHV) scanning tunneling microscope (VT-STM) system with a base pressure of  $1 \times 10^{-10}$  mbar. All STM images were acquired in constant-current mode at the room temperature. HOPG substrates were prepared by cleaving with adhesive tape followed by annealing at approximately 330 °C in the UHV chamber for 3 hours. HATP molecules (purchased from CHEMSOON, purity: 95%) were sublimed at 310 °C using an organic-beam evaporator. Ni(acac)<sub>2</sub> precursors (purchased from Bio-Dream, purity: 96%) were sublimed at 60 °C using the same method. The integrity of the Ni(acac)<sub>2</sub> precursors was checked with deposition on a Au(111) substrate (Figure S7).

## **Acknowledgement**

The work was supported by the Hong Kong RGC 16300425.

## **Author Contributions**

C. S and Y. F. contributed to designing the method, conducting the experiments, acquiring and analyzing the data, and preparing the manuscript. H. C. contributed to designing the method. C. S and N. L contributed to writing the manuscript. N. L. supervised the project. All authors have given approval to the final version of the manuscript.

### **Competing interests**

---

The authors declare no competing interests.

### **Data Availability Statement**

---

The datasets generated during and/or analysed during the current study are available from the corresponding author on reasonable request.

## References:

- (1) T.R. Cook, Y.R. Zheng, P.J. Stang, Metal–organic frameworks and self-assembled supramolecular coordination complexes: comparing and contrasting the design, synthesis, and functionality of metal–organic materials, *Chem. Rev.* 113 (2012) 734–777
- (2) J. Holliday, C.A. Mirkin, Strategies for the construction of supramolecular compounds through coordination chemistry, *Angew. Chem. Int. Ed.* 40 (2001) 2022–2043
- (3) B. Moulton, M.J. Zaworotko, From molecules to crystal engineering: supramolecular isomerism and polymorphism in network solids, *Chem. Rev.* 101 (2001) 1629–1658
- (4) O.M. Yaghi, M. O’Keeffe, N.W. Ockwig, H.K. Chae, M. Eddaoudi, J. Kim, Reticular synthesis and the design of new materials, *Nature* 423 (2003) 705–714
- (5) S. Kitagawa, R. Kitaura, S.I. Noro, Functional porous coordination polymers, *Angew. Chem. Int. Ed.*, 43 (2004), pp. 2334-2375, 10.1002/anie.200300610
- (6) Wang, M.; Dong, R.; Feng, X. Two-dimensional conjugated metal–organic frameworks (2D c-MOFs): chemistry and function for MOFtronics. *Chem. Soc. Rev.* 2021, 50 (4), 2764– 2793
- (7) Zhao, M.; Huang, Y.; Peng, Y.; Huang, Z.; Ma, Q.; Zhang, H. Two-dimensional metal–organic framework nanosheets: synthesis and applications. *Chem. Soc. Rev.* 2018, 47 (16), 6267– 6295
- (8) Clough, A. J.; Yoo, J. W.; Mecklenburg, M. H.; Marinescu, S. C. Two-Dimensional Metal–Organic Surfaces for Efficient Hydrogen Evolution from Water. *J. Am. Chem. Soc.* 2015, 137 (1), 118– 121
- (9) Sheberla, D.; Sun, L.; Blood-Forsythe, M. A.; Er, S.; Wade, C. R.; Brozek, C. K.; Aspuru-Guzik, A.; Dincž, M. High Electrical Conductivity in Ni<sub>3</sub>(2,3,6,7,10,11-hexaiminotriphenylene)<sub>2</sub>, a Semiconducting Metal–Organic Graphene Analogue. *J. Am. Chem. Soc.* 2014, 136, 8859
- (10) Kambe, T.; Sakamoto, R.; Kusamoto, T.; Pal, T.; Fukui, N.; Hoshiko,

- K.; Shimojima, T.; Wang, Z.; Hirahara, T.; Ishizaka, K.; Hasegawa, S.; Liu, F.; Nishihara, H. Redox Control and High Conductivity of Nickel Bis(dithiolene) Complex  $\pi$ -Nanosheet: A Potential Organic Two-Dimensional Topological Insulator. *J. Am. Chem. Soc.* 2014, 136, 14357
- (11) Huang, X.; Sheng, P.; Tu, Z.; Zhang, F.; Wang, J.; Geng, H.; Zou, Y.; Di, C.; Yi, Y.; Sun, Y.; Xu, W.; Zhu, D. A Two-Dimensional  $\pi$ -d Conjugated Coordination Polymer with Extremely High Electrical Conductivity and Ambipolar Transport Behaviour. *Nat. Commun.* 2015, 6, 7408
- (12) Chen, I.-F.; Lu, C.-F.; Su, W.-F. Highly Conductive 2D Metal–Organic Framework Thin Film Fabricated by Liquid–Liquid Interfacial Reaction Using One-Pot-Synthesized Benzenehexathiols. *Langmuir* 2018, 34, 15754
- (13) Xie, L. S.; Skorupskii, G.; Dincă, M. Electrically Conductive Metal–Organic Frameworks. *Chem. Rev.* 2020, 120, 8536– 8580
- (14) Huang, X.; Zhang, S.; Liu, L.; Yu, L.; Chen, G.; Xu, W.; Zhu, D. Superconductivity in a Copper(II)-Based Coordination Polymer with Perfect Kagome Structure. *Angew. Chem., Int. Ed.* 2018, 57, 146
- (15) Zhang, X.; Zhou, Y.; Cui, B.; Zhao, M.; Liu, F. Theoretical Discovery of a Superconducting Two-Dimensional Metal–Organic Framework. *Nano Lett.* 2017, 17, 6166
- (16) Wang, Z.; Liu, Z.; Liu, F. Organic Topological Insulators in Organometallic Lattices. *Nat. Commun.* 2013, 4, 1471
- (17) Crasto De Lima, F.; Ferreira, G. J.; Miwa, R. H. Layertronic Control of Topological States in Multilayer Metal–Organic Frameworks. *J. Chem. Phys.* 2019, 150, 234701
- (18) Zhang, J.; Zhao, B.; Ma, C.; Yang, Z. Prediction of Intrinsic Two-Dimensional Non-Dirac Topological Insulators in Triangular Metal–Organic Frameworks. *Appl. Phys. Lett.* 2019, 114, 043102
- (19) Jiang, W.; Zhang, S.; Wang, Z.; Liu, F.; Low, T. Topological Band Engineering of Lieb Lattice in Phthalocyanine-Based Metal–Organic Frameworks. *Nano*

- Lett. 2020, 20, 1959
- (20) Silveira, O. J.; Ribeiro, G. A. S.; Chacham, H. Activation of Topological Insulator Phase in Kagomé-Type Bilayers by Interlayer Coupling: the Cases of Ni(CO)<sub>4</sub> and Pd(CO)<sub>4</sub>. *Appl. Phys. Lett.* 2020, 116, 103103
- (21) Gao, Y.; Zhang, Y.-Y.; Sun, J.-T.; Zhang, L.; Zhang, S.; Du, S. Quantum Anomalous Hall Effect in Two-Dimensional Cu-Dicyanobenzene Coloring-Triangle Lattice. *Nano Res.* 2020, 13, 1571
- (22) Zhao, M.; Wang, A.; Zhang, X. Half-Metallicity of A Kagome Spin Lattice: the Case of a Manganese Bis-Dithiolene Monolayer. *Nanoscale* 2013, 5, 10404–10408
- (23) Zhang, X.; Zhao, M. Robust Half-Metallicity and Topological Aspects in Two-Dimensional Cu-TPyB. *Sci. Rep.* 2015, 5, 14098
- (24) Jin, Y.; Chen, Z.; Xia, B.; Zhao, Y.; Wang, R.; Xu, H. Large-Gap Quantum Anomalous Hall Phase in Hexagonal Organometallic Frameworks. *Phys. Rev. B* 2018, 98, 057202
- (25) Zhang, L.-C.; Zhang, L.; Qin, G.; Zheng, Q.-R.; Hu, M.; Yan, Q.-B.; Su, G. Two-Dimensional Magnetic Metal–Organic Frameworks with the Shastry-Sutherland Lattice. *Chem. Sci.* 2019, 10, 10381
- (26) Yamada, M. G.; Fujita, H.; Oshikawa, M. Designing Kitaev Spin Liquids in Metal-Organic Frameworks. *Phys. Rev. Lett.* 2017, 119, 057202
- (27) Dong, R., Pfeiffermann, M., Liang, H., Zheng, Z., Zhu, X., Zhang, J., & Feng, X. (2015). Large-area, free-standing, two-dimensional supramolecular polymer single-layer sheets for highly efficient electrocatalytic hydrogen evolution. *Angewandte Chemie International Edition*, 54(41), 12058-12063.
- (28) Dong L, Gao Z A, Lin N. Self-assembly of metal–organic coordination structures on surfaces[J]. *Progress in Surface Science*, 2016, 91(3): 101-135
- (29) Liu, J.; Abel, M.; Lin, N. On-Surface Synthesis: A New Route Realizing Single-Layer Conjugated Metal–Organic Structures. *J. Phys. Chem. Lett.* 2022, 13 (5), 1356–1365

- (30) Li, J.; Solianyik, L.; Schmidt, N.; Baker, B.; Gottardi, S.; Lopez, J. C. M.; Enache, M.; Monjas, L.; van der Vlag, R.; Havenith, R. W. A.; Hirsch, A. K. H.; Stöhr, M. Low-Dimensional Metal–Organic Coordination Structures on Graphene. *J. Phys. Chem. C* 2019, 123, 12730
- (31) Yan, L.; Silveira, O. J.; Alldritt, B.; Krejčí, O.; Foster, A. S.; Liljeroth, P. Synthesis and Local Probe Gating of a Monolayer Metal–Organic Framework. *Adv. Funct. Mater.* 2021, 31, 2100519
- (32) Kumar, A.; Banerjee, K.; Foster, A. S.; Liljeroth, P. Two-Dimensional Band Structure in Honeycomb Metal–Organic Frameworks. *Nano Lett.* 2018, 18, 5596
- (33) Urgel, J. I.; Schwarz, M.; Garnica, M.; Stassen, D.; Bonifazi, D.; Ecija, D.; Barth, J. V.; Auwärter, W. Controlling Coordination Reactions and Assembly on A Cu(111) Supported Boron Nitride Monolayer. *J. Am. Chem. Soc.* 2015, 137, 2420–2423
- (34) Lowe, B.; Field, B.; Hellerstedt, J.; Ceddia, J.; Nourse, H. L.; Powell, B. J.; Medhekar, N. V.; Schiffrin, A. Local Gate Control of Mott Metal-Insulator Transition in a 2D Metal–Organic Framework. *Nat. Commun.* 2024, 15, 3559
- (35) Yan, L.; Silverira, O. J.; Alldritt, B.; Kezilebieke, S.; Foster, A. S.; Liljeroth, P. Two-Dimensional Metal–Organic Framework on Superconducting NbSe<sub>2</sub>. *ACS Nano* 2021
- (36) Lyu, C., Gao, Y., Zhou, K., Hua, M., Shi, Z., Liu, P. N., ... & Lin, N. (2024). On-Surface Self-Assembly Kinetic Study of Cu-Hexaazatriphenylene 2D Conjugated Metal–Organic Frameworks on Coinage Metals and MoS<sub>2</sub> Substrates. *ACS nano*, 18(30), 19793-19801.
- (37) Chen, H., Chen, Y., Mo, S., Li, E., Gao, Y., Huang, L., ... & Lin, N. (2026). Visualizing Interfacial Charge Trapping in a Heterostructure of a Monolayer Metal–Organic Framework on a van der Waals Substrate. *Journal of the American Chemical Society*.
- (38) Liu, J., Chen, Y., Feng, X., & Dong, R. (2022). Conductive 2D conjugated metal–organic framework thin films: synthesis and functions for (opto-)

- electronics. *Small Structures*, 3(5), 2100210.
- (39) Liu, J., Fu, S., Fu, Y., Chen, Y., Tadayon, K., Hambsch, M., ... & Dong, R. (2025). Ammonia-assisted chemical vapor deposition growth of two-dimensional conjugated coordination polymer thin films. *Journal of the American Chemical Society*, 147(21), 18190-18196.
- (40) Lewis, F. D., Salvi, G. D., Kanis, D. R., & Ratner, M. A. (1993). Electronic structure and spectroscopy of nickel (II), palladium (II), and platinum (II) acetylacetonate complexes. *Inorganic Chemistry*, 32(7), 1251-1258.
- (41) Weiss, T., Warneke, J., Zielasek, V., Swiderek, P., & Bäumer, M. (2016). XPS study of thermal and electron-induced decomposition of Ni and Co acetylacetonate thin films for metal deposition. *Journal of Vacuum Science & Technology A*, 34(4).
- (42) Gao, Z. A., Hsu, C. H., Liu, J., Chuang, F. C., Zhang, R., Xia, B., ... & Lin, N. (2019). Synthesis and characterization of a single-layer conjugated metal–organic structure featuring a non-trivial topological gap. *Nanoscale*, 11(3), 878-881.
- (43) Zhao, B., Zhang, J., Feng, W., Yao, Y., & Yang, Z. (2014). Quantum spin Hall and Z<sub>2</sub> metallic states in an organic material. *Physical Review B*, 90(20), 201403.
- (44) Sheberla, D., Sun, L., Blood-Forsythe, M. A., Er, S., Wade, C. R., Brozek, C. K., ... & Dincă, M. (2014). High electrical conductivity in Ni<sub>3</sub>(2, 3, 6, 7, 10, 11-hexaiminotriphenylene)<sub>2</sub>, a semiconducting metal–organic graphene analogue. *Journal of the American Chemical Society*, 136(25), 8859-8862.
- (45) Gu, F., Shu, S., Patrick, C. E., & Castell, M. R. (2024). Scanning tunneling microscopy of bimetallic Ni/Co-HITP metal–organic framework monolayers. *The Journal of Physical Chemistry C*, 128(41), 17797-17805.

Supporting information:

**In vacuo synthesis of single-layer Ni<sub>3</sub>(HITP)<sub>2</sub> on HOPG surface using  
metallo-organic precursor**

Chuyu Song<sup>†</sup>, Yifei Feng<sup>†</sup>, Henan Chen, Nian Lin\*

Department of Physics, The Hong Kong University of Science and Technology, Clear  
Water Bay, Hong Kong 999077, China

<sup>†</sup>These authors contributed equally to this work

\*Corresponding author: [phnlin@ust.hk](mailto:phnlin@ust.hk)

The supplementary materials contain the large scale STM topographs of step (iii) and step (v) in the multi-step growth, Fast Fourier Transform (FFT) pattern of the Ni<sub>3</sub>(HITP)<sub>2</sub> single layer, aggregation behavior of metallic nickel and Ni(acac)<sub>2</sub> on HOPG, different controlled growth experiments, evolution of coordination structures formed with Ni(acac)<sub>2</sub> with HATP molecules on Au(111) surface, thermal and chemical stability of Ni<sub>3</sub>(HITP)<sub>2</sub> single layer, and the structure of Ni(acac)<sub>2</sub> formed on Au(111).

**Figure S1: Large scale STM topographs of step (iii) and step (v) in the multi-step growth.**

At step (iii), the  $\text{Ni}(\text{acac})_x$  clusters are 6.0-7.0 nm in size (measured by the full width at half maximum of the cluster profile) and 2.5-3.5 nm in height. At step (vi), the  $\text{Ni}(\text{acac})_x$  clusters are 5.0-5.5 nm in size (measured by the full width at half maximum of the cluster profile) and 1.5-2.0 nm in height.

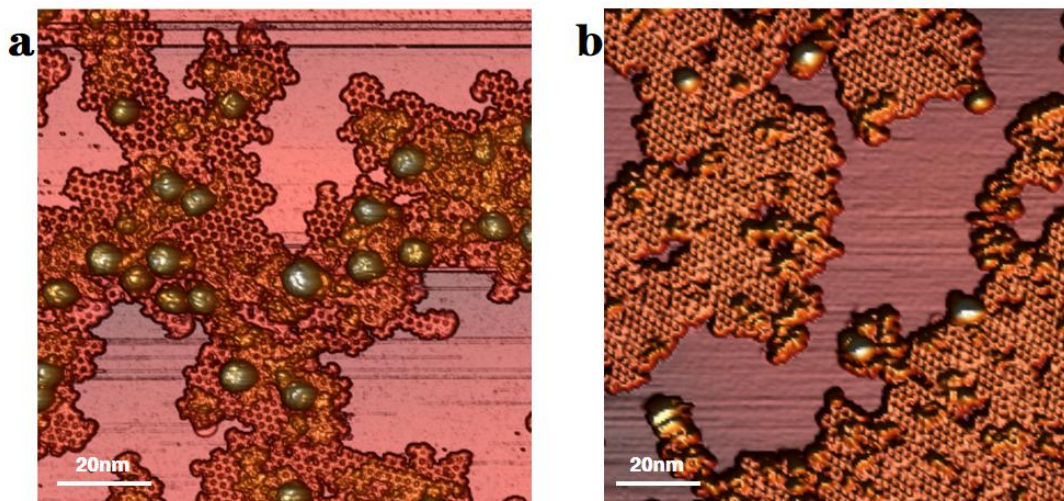


Figure S1. (a) Large scale STM topograph (3D top view) of step (iii). (b) Large scale STM topograph (3D top view) of step (v). Scanning parameters:  $V = -2 \text{ V}$ ,  $I = 500 \text{ pA}$ .

**Figure S2: Fast Fourier Transform (FFT) pattern of the STM image showing different domains of the  $\text{Ni}_3(\text{HITP})_2$  single layer.**

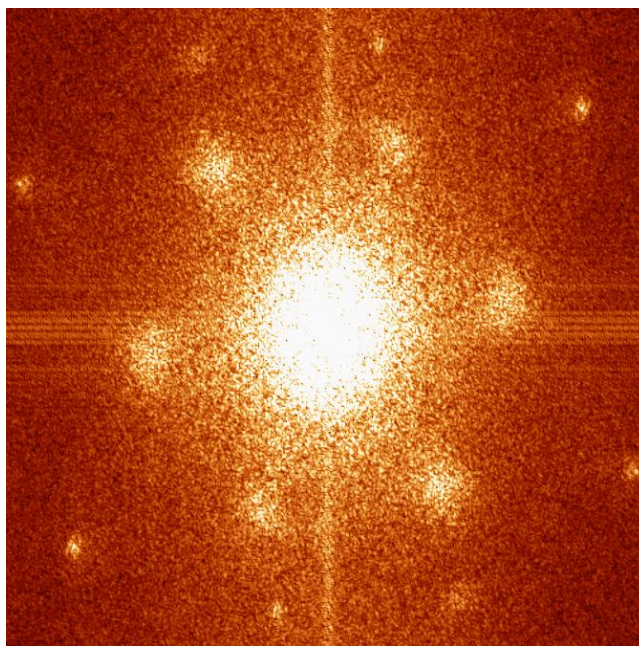


Figure S2. FFT of Figure S1(b) showing the different domains are in the same

orientation.

**Figure S3: Aggregation behavior of metallic nickel and Ni(acac)<sub>2</sub> on HOPG.**

Figure S3b shows Ni atoms aggregate into large clusters after 150 °C annealing, typically 5-7 nm in height and 8-10 nm in lateral size. These clusters predominantly adhere to step edges of the HOPG substrate. In contrast, after 150 °C annealing Ni(acac)<sub>2</sub> form smaller clusters of ~3 nm in height and ~3 nm in lateral size. These clusters aggregate on the open terraces of the HOPG substrate.

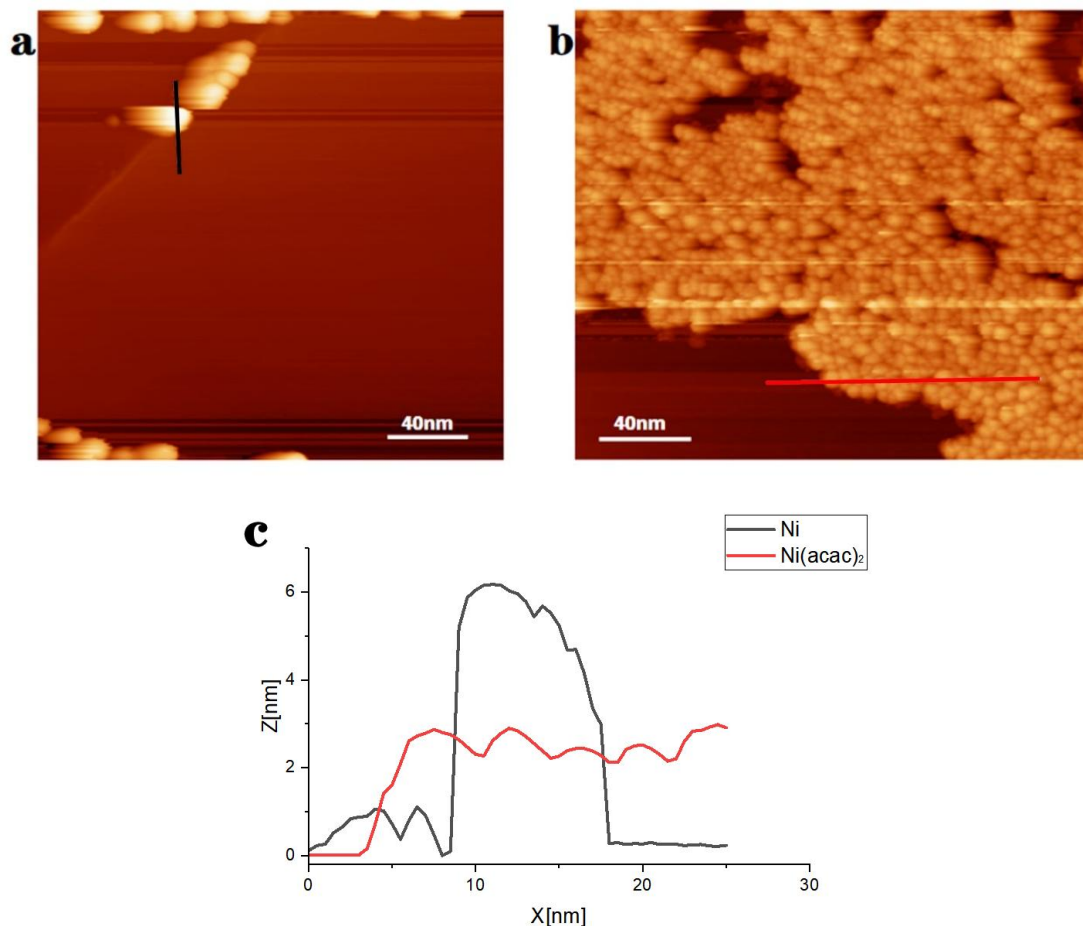


Figure S3. (a) STM topograph showing large Ni atom clusters formed on HOPG. (b) STM topograph showing small Ni(acac)<sub>2</sub> clusters formed on HOPG. (c) Height profiles of the lines indicated in (a) and (b) showing the contrast of the cluster size of the two samples. Scanning parameters: V= -2V, I= 500 pA.

**Figure S4: Co-deposition of HATP and Ni(acac)<sub>2</sub> on HOPG held at high temperature (~300 °C).**

Depositing HATP and Ni(acac)<sub>2</sub> on the hot substrate yields small pieces of Ni<sub>3</sub>(HITP)<sub>2</sub> formed at the step edge of the HOPG. Presumably, both HATP and Ni(acac)<sub>2</sub> desorb from the hot substrate, preventing the formation of large Ni<sub>3</sub>(HITP)<sub>2</sub> domains.

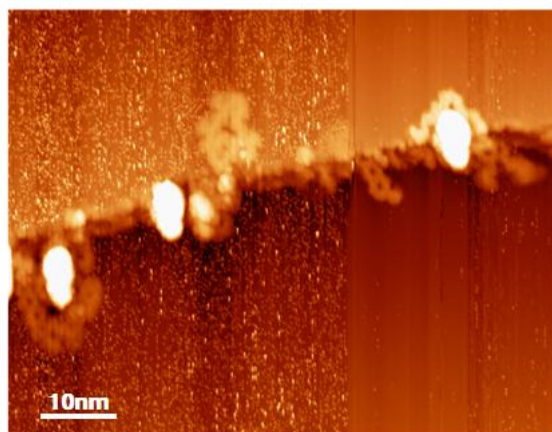


Figure S4. STM topograph showing small pieces of  $\text{Ni}_3(\text{HITP})_2$  at the step edge of the HOPG substrate formed by co-deposition of HATP and  $\text{Ni}(\text{acac})_2$  simultaneously onto a hot HOPG substrate. Scanning parameters:  $V = -2\text{V}$ ,  $I = 500\text{ pA}$ .

**Figure S5: Evolution of coordination structures formed with  $\text{Ni}(\text{acac})_2$  and HATP molecules on Au(111) surface.**

Co-deposition of HATP and  $\text{Ni}(\text{acac})_2$  onto Au(111) at room temperature does not yield any ordered structures. Upon subsequent annealing (Figure S5 a–d), coordination structures are formed, suggesting Ni ions are released. At  $150^\circ\text{C}$ , small, short coordination oligomers such as dimers and trimers are formed. As the annealing temperature increases to  $250^\circ\text{C}$ , longer coordination chains and hexagonal rings are formed. At  $300^\circ\text{C}$ , small patches of  $\text{Ni}_3(\text{HITP})_2$  are formed. A one-step annealing at  $300^\circ\text{C}$  yields slightly larger  $\text{Ni}_3(\text{HITP})_2$  domains. However, these domains are much smaller than those formed on HOPG.

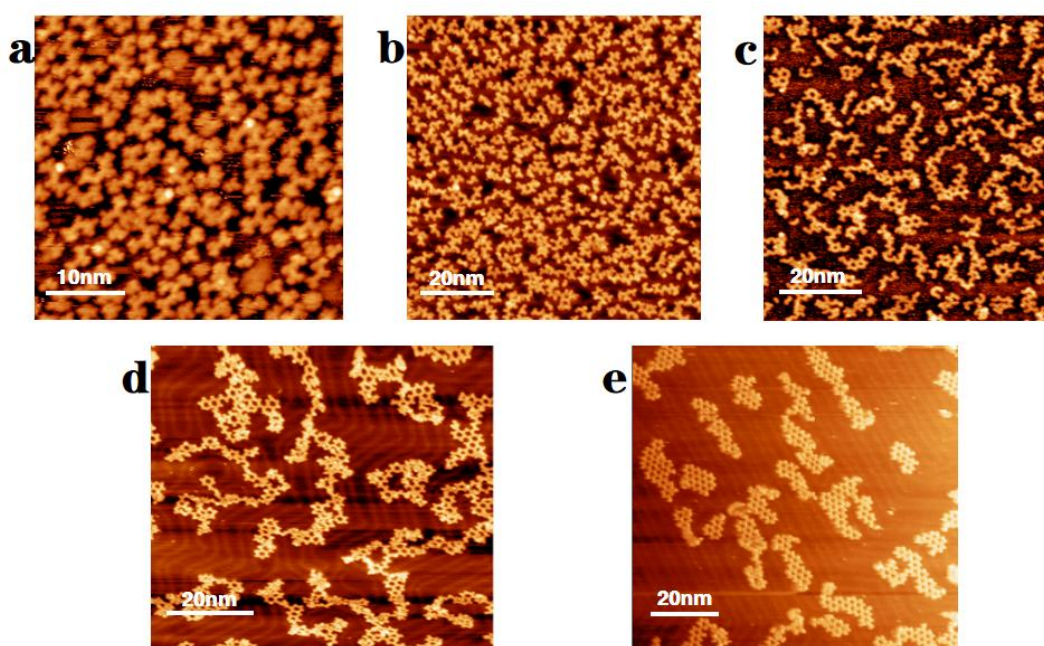


Figure S5. (a-d) Coordination structures formed with  $\text{Ni}(\text{acac})_2$  and HATP on Au(111)

subjected to stepwise annealing at different temperatures. (a) 150°C. (b) 200°C. (c) 250°C. (d) 300°C. (e): One-step annealing at 300°C without intermediate annealing steps. Scanning parameters:  $V = -2\text{V}$ ,  $I = 500\text{ pA}$ .

**Figure S6: Thermal and chemical stability of  $\text{Ni}_3(\text{HITP})_2$  single layers formed on HOPG.**

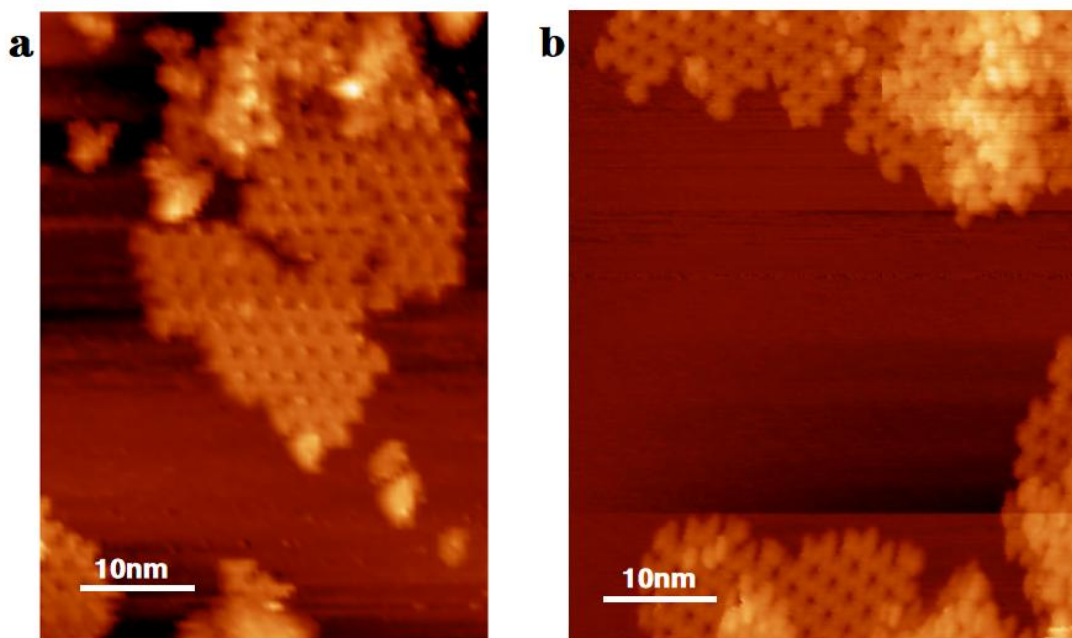


Figure S6. STM topographs showing the sample subjected to: (a) annealing at 350°C for 10 minutes. (b) exposure to ambient air for 30 minutes, re-introducing the sample back to vacuum and annealing at 150°C. Scanning parameters:  $V = -2\text{ V}$ ,  $I = 500\text{ pA}$ .

**Figure S7: Structure of  $\text{Ni}(\text{acac})_2$  formed on Au(111).**

Figure S7a shows that  $\text{Ni}(\text{acac})_2$  deposited on Au(111) form closely packed one-dimensional chains. The high-resolution image of Figure 7b features that the chains are composed of periodically ranged unit with a lattice constant of 8.8 Å. This lattice constant matches the size of  $\text{Ni}(\text{acac})_2$  complex, as shown in the overlaid molecular model in Figure 7b.

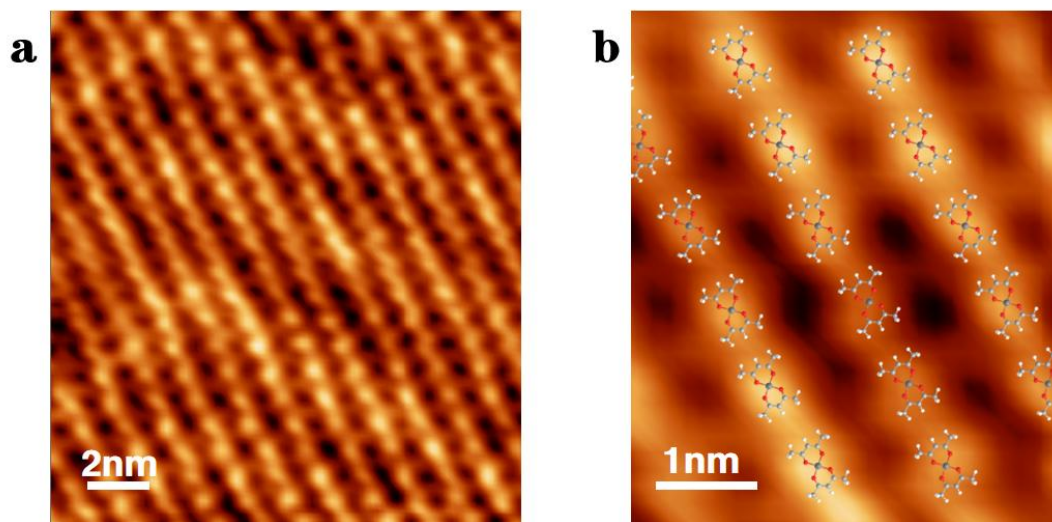


Figure S7. (a) Closely packed one-dimensional chains formed out of Ni(acac)<sub>2</sub> on Au(111) surface. (b) The periodical lattice matching the size of Ni(acac)<sub>2</sub> as illustrated by the overlaid molecular model.